Mon. Not. R. Astron. Soc. **000**, 1–?? (0000) Printed 12 June 2002 (MN LaTeX style file v1.4)

The symbiotic star CH Cygni. IV. Basic kinematics of the circumstellar matter during active phases

A. Skopal[1⋆], M.F. Bode[2], M.M. Crocker[3], H. Drechsel[4], S.P.S. Eyres[5] and R. Komžík[1]

[1] *Astronomical Institute, Slovak Academy of Sciences, 059 60 Tatranská Lomnica, Slovakia*
[2] *Astrophysics Research Institute, Liverpool John Moores University, Twelve Quays House, Egerton Wharf, Birkenhead CH41 1LD, UK*
[3] *Jodrell Bank Observatory, University of Manchester, Manchester, Macclesfield, Cheshire, SK11 9DL, UK*
[4] *Dr.-Remeis-Observatory Bamberg, University of Erlangen-Nürnberg, Sternwartstrasse 7, D-96049 Bamberg, Germany*
[5] *Centre of Astrophysics, University of Central Lancashire, Preston, PR1 2HE, UK*

Received; in original form

ABSTRACT

We give a brief summary of common basic characteristics of active phases during the whole (1963-2000) observed symbiotic life of CH Cygni. We identify two types of outbursts: (1) Those with pronounced signatures of a high-velocity mass outflow, and (2) those displaying signatures of only a mass inflow to the central star. On the basis of the observed Hα emission, we investigate mass loss from the active star during the period from when radio jets appeared (1984.6) to the most recent activity (1998-00). A simple expression, which relates the observed Hα luminosity to the mass-loss rate, is derived. We obtained mass-loss rates of $\dot{M} = 4.4 \pm 1.5$, ≈ 2.0 and $1.8 \pm 0.7 \times 10^{-6}\, M_{\odot}\mathrm{yr}^{-1}$ in 1984 October, 1992 August and 1998 September, respectively. Our values are in very good agreement with radio mass-loss rates determined previously. Mass loss from CH Cygni is a transient effect connected only with active phases of type (1), and is very variable. The ejected material, which is accelerated to the same v_{∞} at a distance of $\approx 100\, R_{\odot}$, is heavily decelerated at much larger distances (≈ 1000 A.U). The most recent ejecta reflect a larger deceleration.

Key words: stars: mass-loss – binaries: symbiotics – stars: individual: CH Cygni

1 INTRODUCTION

CH Cygni is a particularly intriguing symbiotic star. It is very bright, with V between about 6 and 9, and well placed in the northern hemisphere ($\delta \sim +50^{\circ}$), which makes it a perfect target for multi-frequency ground-based observations. Despite this advantage, the nature of its activity, and even its fundamental parameters, are poorly known. The following are significant dates, which moved ahead our understanding of the CH Cygni phenomenon:

In 1979, after 16 years of intensive observations from the beginning of activity, Yamashita & Maehara (1979) succeeded in searching for a reliable periodicity in radial velocities in the red spectrum. They suggested the binary model for CH Cyg, consisting of a red giant and a white dwarf with an orbital period of 5 700 days. In the 1980s the elements of the binary model were improved (e.g. Mikolajewski et al. 1987) and confirmed by the radial velocity curve for the active component (e.g. Hack et al. 1986, Skopal, Mikolajewski & Biernikowicz 1989). A new avenue in the investigation of CH Cyg was set by Hinkle et al. (1993) who suggested a triple-star model on the basis of precise radial velocity measurements in the infrared spectrum. The triple-star model was confirmed and modified by identifying eclipses in the system (Skopal 1995, Skopal et al. 1996a, Iijima 1998). Further confirmation was provided by Skopal et al. (1998b), who measured radial velocities of the active star from high-resolution IUE spectra corresponding to its orbital motion in the suggested short-period inner binary. Finally, the distance to CH Cygni was determined on the basis of Hipparcos measurements as 270 ± 66 pc (Viotti et al. 1997). Based on these studies, we investigate CH Cygni as a triple-star system consisting of the inner, 756-day period, symbiotic binary, which is moving in a common orbit with another red giant with a 5300-day period orbit.

In this paper we give a concise summary of basic characteristics, which are common to all active phases. In Sect. 2

⋆ Visiting Astronomer: Astrophysics Research Institute, Liverpool; Astronomical Institute, Bamberg

we identify two types of outbursts with respect to mass outflow and/or infall from/to the central object. In Sect. 3 we introduce a simple Hα method to investigate mass-loss rate during active stages, and in Sect. 4 we discuss the derived and observed properties of the mass outflow.

2 OBSERVATIONS

Summarising variations in (mainly) hydrogen line profiles in the spectrum of CH Cygni during its whole period of symbiotic life (from 1964 to date), we can recognise two types of active phases:

(1) Those with pronounced signatures of the high-velocity mass *outflows*, such as P-Cygni type profiles and very extended emission wings. The basic kinematics of the circumstellar matter reflected motions from the active star.

(2) Others displaying pronounced *inverse* P-Cygni type of line profiles indicating a mass *infall* to the central star. The basic kinematics of the circumstellar matter corresponded to an accretion process.

Phases of activity, 1967-70, 1992-95 and 1998-00, belong to the first type. In spite of very heterogenous data (in quality, coverage and presentation), all these relatively short-term active episodes exhibited strong absorptions of the P-Cygni type and/or very extended emission wings in hydrogen Balmer lines. It is probable that it was also the case in the first detected appearance of CH Cyg activity in 1963-65. However, there was only one report made by Deutsch (1964) saying that in 1963 September CH Cyg showed a composite spectrum with strong and wide emissions of H I. For the 1967-70 activity it was shown best by Doan (1970), who presented a strong blueward absorption in Hβ during 1967-69 (see his Fig. 4). Also features seen redward from the reference line on Doan's spectra suggest some similarities with those observed during recent phases of activity. The authors during that time presented only parts of the line profiles displaced by about $\pm$10 Å around the reference line, which does not allow one to evaluate the extension of the emission wings. The 1992-95 activity started with the appearance of P-Cygni type of hydrogen profiles (Skopal, Hric & Komžík 1992) and an extension of the emission in the line wings to about $\pm$ 2 000 km s^{-1}was reported by other authors (e.g. Tomov et al. 1996, Skopal et al. 1996b). Similar features were observed also in the recent, 1998-00, active phase (Eyres et al. 2002, this paper).

In contrast, during the main active phase, 1977-1984.6, (with respect to the star's brightness and its duration), no signatures of comparable mass outflow were indicated. Only at the very beginning of the outburst, in 1977 September, a faint absorption at $\approx$-300 km s^{-1}in Hγ could be seen (Hack et al. 1988), and Anderson et al. (1980) detected an emission blob in Hα at $\approx$-150 km s^{-1}on 1979 May. From Summer of 1981, pronounced *inverse* P-Cygni profiles developed and dominated the basic characteristics of the line spectrum until 1984 July (e.g. Hack et al. 1988). We take this as evidence of mass *infall* to the central star. Representative examples are plotted in Figs. 1 and 2. Therefore this period of activity belongs to type (2). The following decline from activity, 1984.6 to $\sim$1988, was characterised by significant expansion of hydrogen emission wings to $\sim \pm$3 000km s^{-1}(Mikolajewski & Tomov 1986, Figs. 1 and 3 in this paper), and thus is consistent with the type (1) active phase. A common property of all active stages was a rapid variability of spectrophotometric parameters (Faraggiana & Hack 1971, Skopal et al. 1989, Tomov et al. 1996, Eyres et al. 2002).

Table 1. Journal of presented observations

Date	Resolution	Region	References
1980 May 6	high	Lyα	3
1981 Aug 7	8Å mm−1	3 600 - 5 000 Å	1
1984 Oct 4	8Å mm−1	3 800 - 6 800 Å	2
1985 Jan 23	high	Lyα	3
1986 Mar 20	5 GHz map	VLA C band	4
1992 Jul 21	17Å mm−1	3 600 - 5 000 Å	5
1992 Aug 11	–	H$_{\alpha,\beta}$	5
1992 Aug 13	–	H$_{\alpha,\beta}$	5
1994 Oct 14	high	Lyα	3
1995 Aug 20	5 GHz map	VLA C band	4
1998 Sep 5	–	4 200 - 6 700 Å	6
1999 Jan 5	–	4 200 - 6 700 Å	6
1999 26 Sep	5 GHz map	VLA C band	4

1 - Skopal (1986), 2 - Skopal et al. (1993), 3 - Skopal et al. (1996b), 4 - Crocker et al. (2001), 5 - Skopal et al. (1988b), 6 - Eyres et al. (2002)

In Figs. 1 and 2 we selected some examples of this evolution. The wavelengths were converted to velocity units relative to $\lambda\lambda$6562.82, 4861.33, 4340.47, 4101.74 and 3889.05 Å respectively for Hα, Hα, Hβ, Hγ, Hδ and H$_8$. Flux calibration of the spectra is described in Appendix A. Other details of observational material used in this contribution are introduced in Table 1 and references therein.

3 ANALYSIS OF HYDROGEN LINE PROFILES

In this section we analyse the high velocity mass-outflow characteristic of type (1) active phases.

Figure 3 shows the bottom parts of hydrogen line profiles typical for the period after 1984.6. They were observed during three individual episodes of activity: 1984.6-1986, 1992-1995 and 1998-2000. The emission wings extending to 2 500-3 500 km s^{-1} represent a common feature of H I line profiles in this period. They are seen best in Hα, but can be recognised also in Hβ, Hγ and Hδ (Fig. 3). No such features were observed during the maximum of activity, 1977-1984.6. During the 1992-1995 and 1998-2000 episodes, rapid variation at both sides of the reference line was observed on a time-scale of days to months. When comparing different profiles, one can recognise that there are (strong) blue- and redward-shifted absorptions, causing the variability near to the central emission, which, as a result, become temporarily very narrow. After a few days/months, the absorption features disappear, and the original broad emission profiles return (Eyres et al. 2002, Fig. 3). Many other details of this behaviour have already been described by other authors (e.g. Tomov et al. 1996).

Figure 3 suggests that the HI profiles are composed of a few main components. To extract them, we fitted the observed profile with 1 to 4 Gaussian functions, according to its complexity. For this purpose we used our own code GAUS,

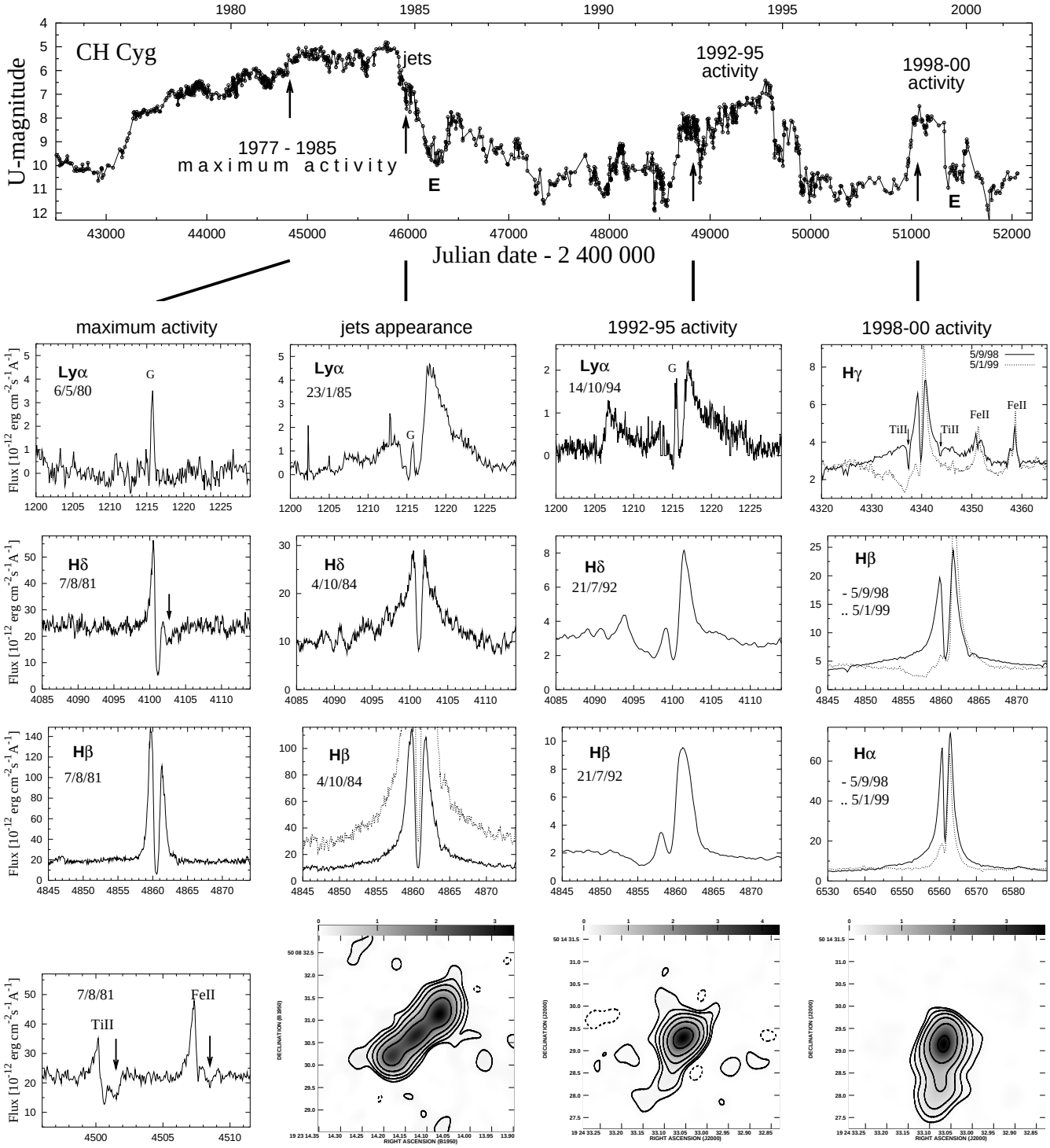

Figure 1. Evolution in selected line profiles during the last four active periods of CH Cyg. From the left to the right columns and connected with the corresponding Julian date, marked in the light curve at the top panel:
(i) The maximum of the star's brightness. A variable infall of about $+100\,\mathrm{km\,s^{-1}}$to the central star was detected (marked by arrows). No clear signatures of a mass outflow were indicated. The circumstellar Lyα was not present (G denotes only its geocoronal component).
(ii) Jet appearance period. A drastic change happened after 1984.6, when the jets in the radio domain were observed. The line profiles displayed a high-velocity outflow. In the optical, absorptions were close to the line centers, while in the ultraviolet P-Cygni profiles were found (see Skopal et al. 1998b for more details).
(iii) The 1992-95 activity. In this period, in addition to the very broad emission wings of hydrogen lines, a complex and variable absorption/emission structure was often observed mainly on the blue side of the line center.
(iv) The 1998-2000 activity. This period was characterised by a similar behaviour as the previous one, but double-peaked hydrogen profiles were often observed (see Eyres et al. 2002 for more details).
The remnants of the mass loss during activity after 1984.6 have unambiguously been detected by the radio VLA imaging (Crocker et al. 2001).

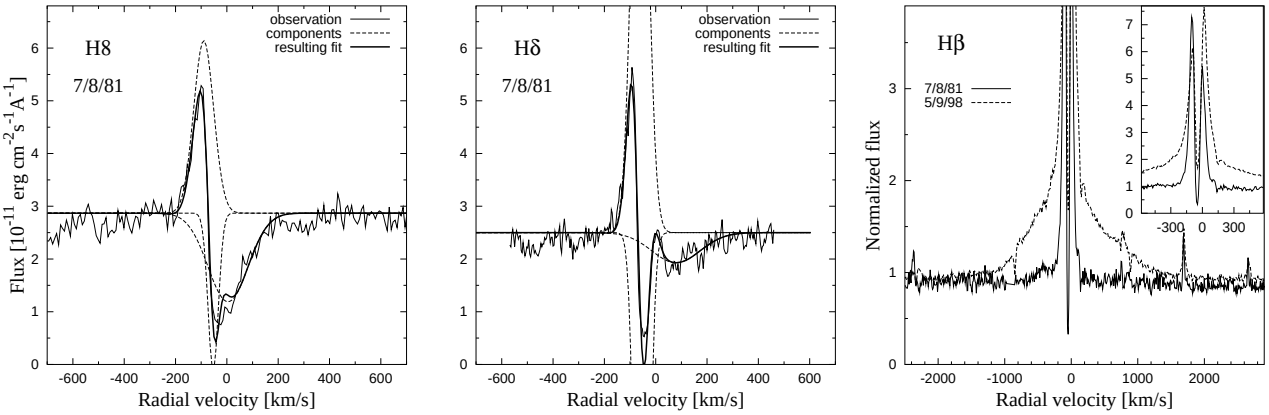

Figure 2. During the maximum of activity a redward shifted absorption was often very pronounced, mainly in the profiles of the higher members of Balmer lines (left and mid panels). Observed radial velocities, running from ~ 0 to $\sim +200 \mathrm{km\,s^{-1}}$, indicated a mass infall to the central star. The space velocity of the system, -58 $\mathrm{km\,s^{-1}}$, even combined with that of the orbital motion, $\sim +15\,\mathrm{km\,s^{-1}}$in 1981 August (cf. Fig. 2 of Skopal et al. 1989), enlarges the relative infall velocity. During the whole period of maximum brightness (1977 May - 1984 June), the very extended emission wings had not been observed prior to 1984.6 (right panel).

which is based on the simplex method. Parameters of individual components are summarised in Table 2 and the results drawn in Figs. 2 and 3. We use these data to determine fluxes of the extended emission components (in Table 2 and Fig. 3 denoted as 'wind component') and their terminal velocities (Table 3). However, during 1992 and also 1984, mainly around the Hα region, the influence of the late-type spectrum on the line profiles makes it difficult to determine the line fluxes accuratelly (Appendix B). In 1992 features of the giant spectrum were rather pronounced, the continuum from the active star was faint and the red wings of the profiles were affected by an absorption (cf. Fig. 3). We therefore had to mirror the blue parts of the 'wind' profiles to match them by a Gauss function. As a result obtained fluxes are only approximate in 1992. Further, the influence of the M spectrum on the Hα line on 4/10/84 is shown in Fig. B3 (Appendix B). Here the gaussian fit defines well the broad 'wind' component of the profile, but the difficulty in calibrating the late-type spectrum accurately enlarges the uncertainty of its flux by about 20%.

In the following section, based on the observed luminosity in the Hα line, we will try to estimate the mass-loss rate from the active star in CH Cygni.

3.1 Mass loss during 1984.6-2000 active phases

In the recombination process, the transition from the third to the second level of hydrogen has a high probability of producing the Hα line in emission. In the case of an ionised stellar wind, the Hα profile contains information on its emissivity and velocity distribution. Thus, having a theoretical Hα luminosity and some knowledge of the velocity field of the outflow, one can derive the mass-loss rate, $\dot{M}$, from the measured strength of the Hα emission. Hα, as a tracer of mass loss from hot stars, has been used by many authors (e.g. Klein & Castor 1978, Leitherer 1988, Lamers & Cassinelli 1999). However, the method has never been used in investigations of symbiotic binaries, although emission in Hα was well detected. An approximative approach to estimate $\dot{M}$ for EG And and AG Peg was used only by Vogel (1993) and Vogel & Nussbaumer (1994). In both cases the authors used emission from the He II 1640Å line, assuming it to be optically thin in a constant velocity wind ($v = v_\infty$).

In spite of differences between an interacting binary and a single hot star, we suggest an application, in which the fundamental assumptions of the use of the Hα method can be applied also in our case.

3.1.1 Hα luminosity of the stellar wind

In our simplified approach we will assume that the wind is (i) spherically symmetric with a steady mass-loss rate $\dot{M}$, (ii) fully ionised and completely optically thin in Hα and (iii) isothermal at the same temperature as the stellar (pseudo)photosphere. Validity of assumption (ii) is supported by the large velocity gradient in the stellar wind, because of its large terminal velocity ($v_\infty \gg v_{\rm th}$, where $v_{\rm th}$ is the thermal velocity). If a line photon, created by recombination in such a wind, has traveled a distance $l > 2v_{\rm th}/(dv/dl)$, where (dv/dl) is the velocity gradient of the wind along the path of the photon, it is Doppler shifted with respect to the surrounding gas by more than $2v_{\rm th}$ and thus cannot be absorbed any more in the same line transition. In such conditions the escape probability of the emitted photons will be close to 1. Then the total line luminosity, $L(\mathrm{H}\alpha)$, is related to the line emissivity of the wind, $\varepsilon_\alpha n_{\rm e} n^+$, by

$$L(\mathrm{H}\alpha) = 4\pi d^2 F(\mathrm{H}\alpha) = \varepsilon_\alpha \int_V n_{\rm e} n^+(r)[1 - w(r)]\,\mathrm{d}V, \qquad (1)$$

where d is the distance to the system, $F(\mathrm{H}\alpha)$ represents the observed flux in Hα ($\mathrm{erg\,cm^{-2}\,s^{-1}}$), $\varepsilon_\alpha = 3.56 \times 10^{-25} \mathrm{erg\,cm^3\,s^{-1}}$ is the volume emission coefficient in Hα (Case B: Gurzadyan 1997). In our approach we neglect a variation of the recombination coefficient throughout the wind due to the variation of electron temperature and, in addition, assume the simplest case of $T_{\rm e} = 10^4$ K (assumption (iii) above). Therefore we took ε_α outside of the integral in Eq. (1). Finally, $n_{\rm e}$ and n^+ are number densities of electrons and ions (protons), and the factor $w(r)$ is the fraction

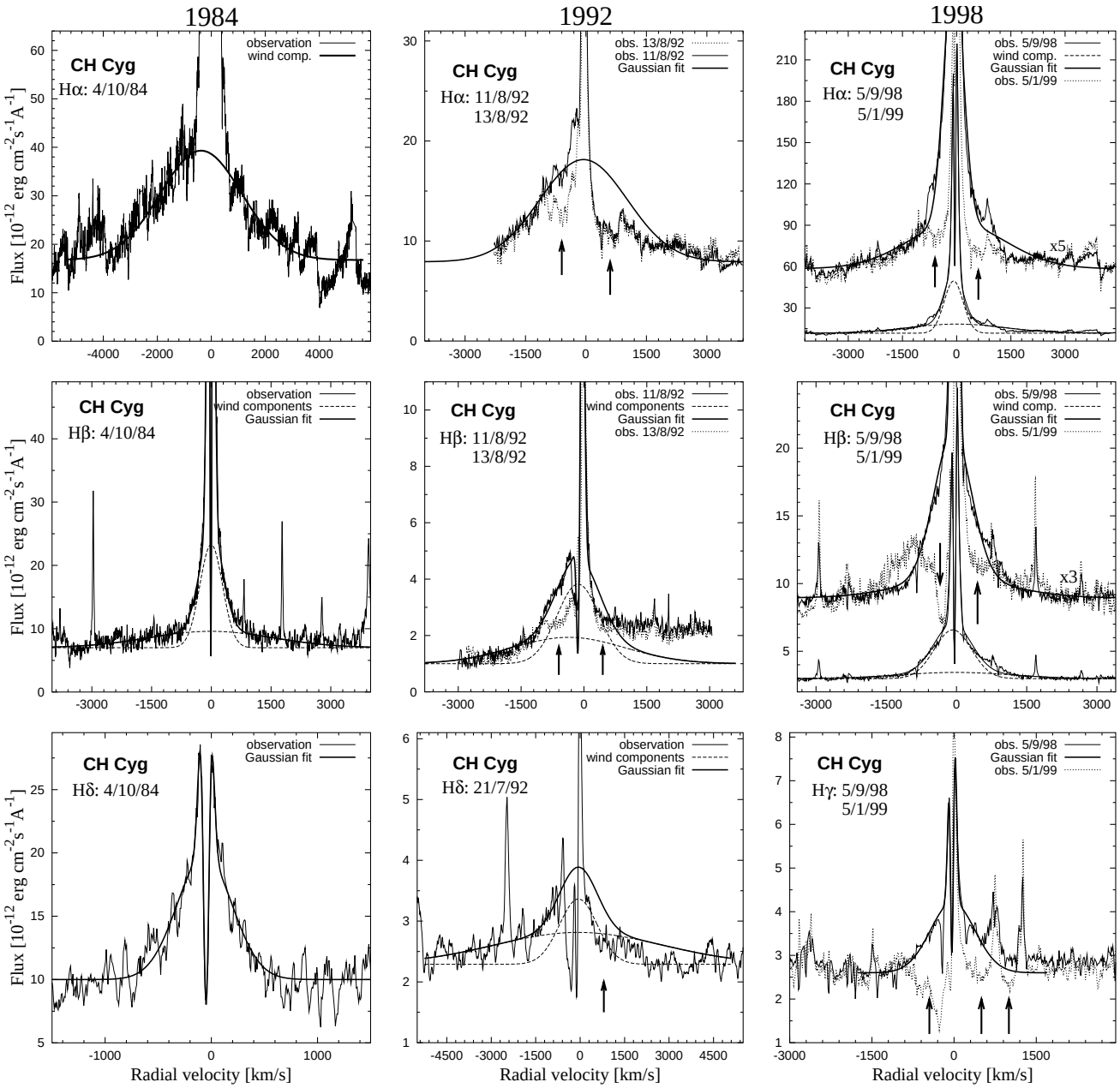

Figure 3. Hydrogen profiles during three active periods. Left column: 1984 - the sudden drop in the star's brightness followed by the radio jet appearance. Terminal velocities reached values of about $\pm 3\,500\,\mathrm{km\,s^{-1}}$ in Hα. Mid column: 1992 - the active phase, 1992-95. The wings were extended to about $\pm 3\,000\,\mathrm{km\,s^{-1}}$. In addition, absorptions on both sides of the line profile at $\pm(400 - 600)\,\mathrm{km\,s^{-1}}$ appeared (marked by arrows). Right column: 1998 - the recent, 1998-2000, activity. Basic signatures of the profiles were similar to those during the 1992-95 activity, but the emission extending to about $\pm 3\,000\,\mathrm{km\,s^{-1}}$ was sometimes located symmetrically with respect to the reference line (Eyres et al. 2002).
Solid thick lines represent the resulting fit of the observed profile by Gaussian functions (parameters in Table 2). Broken lines are the broad components of the profile (if more than 1 Gauss function was used) and denoted in panels as 'wind components'.

of the solid angle that is covered by the photosphere. The value of $w(r)$ is given by

$$w(r) = \frac{1}{2} - \frac{1}{2}\left[1 - \left(\frac{r_{\min}}{r}\right)^2\right]^{1/2}, \qquad (2)$$

where $r_{\min}$ is a distance from the stellar centre where the optical depth in the line becomes small (<1, i.e. the integration can start at this point). Usually this is considered to be equal to the stellar radius, $R_\star$. In our case, $r_{\min} > R_\star$, because of the presence of very strong central absorption component in the observed profile (here Figs. 1, 2, 3, Table 2), which follows the orbital motion of the active star in CH Cyg (Skopal et al. 1989). This reflects the presence of an optically thick layer above the stellar radius (represented here by a pseudophotosphere of a few solar radii which develops during active phases), within which equation (1) is not valid. Below we show that w represents a small correction factor, if the volume integration is carried out to large distances from the centre. For a completely ionised medium,

Table 2. Parameters of Gaussian fits to hydrogen lines

Component	Intensity†	λ_0[Å]	$\sigma_{\rm obs}$	Flux‡
Hβ: 7/8/1981				
Central emission	254.1	4860.45	0.74	469
Central absorption	-293.1	4860.54	0.39	–
Hδ: 7/8/1981				
Central emission	101.4	4100.90	0.43	109
Central absorption	-118.5	4101.01	0.33	–
Redward absorption	-5.7	4102.82	1.28	–
H$_8$: 7/8/1981				
Central emission	32.7	3887.88	0.51	41.4
Central absorption	-29.9	3888.36	0.26	–
Redward absorption	-16.8	3889.11	1.01	–
Hα: 4/10/1984				
Wind emission 2	21.0	6559.48	33.13	1670
Hβ: 4/10/1984				
Central emission	148.6	4861.11	1.10	406
Central absorption	-169.8	4861.14	0.45	–
Wind emission 1	16.3	4861.28	4.63	189
Wind emission 2	2.6	4861.12	25.30	163
Hδ: 4/10/1984				
Central emission	49.4	4099.25	0.57	70.1
Central absorption	-61.2	4099.25	0.42	–
Wind emission 1	9.8	4099.05	3.54	86.8
Hα: 11/8/1992*				
Wind emission 2	10.2	6561.50	23.8	610:
Hβ: 11/8/1992*				
Central emission	58.6	4859.91	0.95	139:
Central absorption	-54.8	4859.67	0.86	–
Wind emission 1	2.8	4859.09	8.16	57.6:
Wind emission 2	0.94	4855.40	21.77	50.6:
Hδ: 21/7/1992*				
Wind emission 1	1.1	4100.91	8.71	23.4:
Wind emission 2	0.52	4100.88	38.5	47.2:
Hα: 5/9/1998				
Central emission	249	6561.92	1.36	852
Central absorption	-240	6561.76	0.54	–
Wind emission 1	37.8	6560.96	5.73	544
Wind emission 2	6.6	6562.87	29.22	483
Hβ: 5/9/1998				
Central emission	29.6	4860.79	0.93	69.2
Central absorption	-32.4	4860.69	0.45	–
Wind emission 1	3.6	4860.07	6.39	57.6
Wind emission 2	0.46	4861.06	19.08	21.8
Hγ: 5/9/1998				
Central emission	11.4	4340.00	0.69	19.6
Central absorption	-12.5	4339.95	0.47	–
Wind emission 1	1.6	4340.11	5.86	23.7

† height of the line in units of 10^{-12} erg cm^{-2} s^{-1} Å^{-1}
‡ in 10^{-12} erg cm^{-2} s^{-1}
$\star$ The fit is valid only for the blue side of the line (Fig. 3)
: Approximate value

($n_{\rm e} \simeq n^+$), the particle density $n(r)$ in the wind can be expressed in terms of the mass loss rate and the velocity law via the mass continuity equation as

$$n(r) = \dot{M}/4\pi r^2 \mu m_{\rm H} v(r), \qquad (3)$$

where μ is the mean molecular weight, $m_{\rm H}$ is the mass of the hydrogen atom and $v(r)$ is the velocity distribution in the hot star wind that we approximate according to the Castor, Abbott & Klein (1975) model by

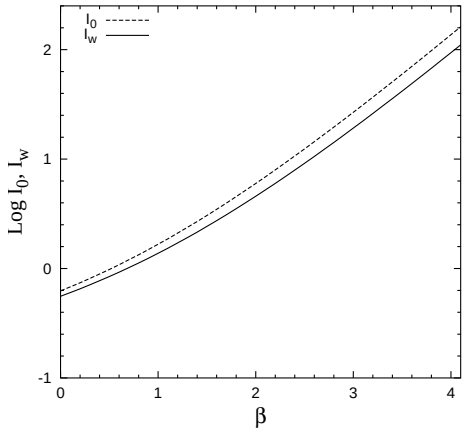

Figure 4. Comparison of integrals $I_{\rm w}$ and I_0 in Eqs. (6) and (7) for $f = R_\star/r_{\rm min} = 5/8$.

$$v(r) = v_\infty \left(1 - \frac{R}{r}\right)^\beta, \qquad (4)$$

in which v_∞ is the terminal velocity of the wind, the distance r is counted from the centre of the star (note that actual integration starts at $r = r_{\rm min}$) and R ($\sim R_\star$) is the origin of the stellar wind. The parameter β characterises an acceleration of the wind. A larger β corresponds to a slower transition to v_∞.

Substitution of Eq. (2) and (3) into Eq. (1) and using dimensionless parameters $x = R_\star/r$ and $f = R_\star/r_{\rm min}$ (i.e. $r_{\rm min}/r = x/f$) yields an expression for the Hα luminosity

$$L({\rm H}\alpha) = \frac{\varepsilon_\alpha}{4\pi(\mu m_{\rm H})^2}\left(\frac{\dot{M}}{v_\infty}\right)^2 \frac{1}{R_\star} \times I_{\rm w}, \qquad (5)$$

where

$$I_{\rm w} = \int_0^f \frac{1/2 + 1/2[1-(x/f)^2]^{1/2}}{(1-x)^{2\beta}} {\rm d}x. \qquad (6)$$

For the case, in which we neglect effects of occultation of the wind material by the stellar disk (i.e. $w(r)$=0), Eq. (6) simplifies to

$$I_0 = \int_0^f \frac{{\rm d}x}{(1-x)^{2\beta}}, \qquad (7)$$

solution of which can be expressed in an analytical form

$$I_0 = \frac{1}{(1-2\beta)}\left[1 - \left(1-f\right)^{1-2\beta}\right] \qquad \text{for } \beta \neq 0.5$$
$$= \ln(1-f) \qquad \text{for } \beta = 0.5. \qquad (8)$$

This integral can also be useful to estimate the emission measure, $\int n_+ n_{\rm e}\, {\rm d}V$, of a fully ionized sphericaly symmetric wind produced by the central star (see Eq. 13 of Skopal 2001). In Fig. 4 we compare both integrals for $f = R_\star/r_{\rm min}$ = 5/8. In the interval of $\beta = 0$ to 3, $I_{\rm w}$ is lower by a factor of ∼20% than I_0. Thus, one can take advantage of the simplicity of Eq. (8) to derive a rough estimate. From the figure it is also obvious that the luminosity $L(\rm H\alpha)$ will critically depend on the parameter β in the wind law. For example, variation of β between 1 and 2 correspondingly scales the luminosity by a factor of 3.3. Therefore, in the following section, we try to estimate the β parameter by comparing a synthetic-line profile to the observed one.

3.1.2 Simple Hα profile of the stellar wind

We assume that the broad components of the hydrogen line profiles (Fig. 3, Table 2) form in an optically *thin* and spherically symmetric stellar wind. In our model the global line profile is assembled by summing the independent Doppler-shifted contributions from each volume element of the expanding material around the central star. The profile thus represents a 'broadening function' resulting from a field of contributions which differ in emissivity and radial velocity and can be compared to only high-velocity features in the profile. The central emission core with a narrow absorption cannot be matched by our approach.

Integration starts from a shell at $r_{\rm min}$ above the pseudophotosphere, $R_\star$. Each geometrically and optically thin shell around the star at distance between r and Δr with expansion velocity $v(r)$ (Eq. 4) produces a flat emission extending from $-v(r)$ to $+v(r)(1-\cos\theta_{\rm min})$ (Fig. 5). Due to very large terminal velocities ($\sim$3 000 km s^{-1}) we neglect the intrinsic broadening by thermal motions. Integration of each shell begins from the direction to the observer ($\theta = 0$) to the angle $\theta = \pi - \theta_{\rm min}$ ($\sin\theta_{\rm min} = r_{\rm min}/r$), beyond which the wind material is occulted by a dense region below the $r_{\rm min}$ radius (see Fig. 5). Volume elements of the same radial velocity, $RV = v(r)\cos\theta$, are represented by annuli around the line of sight, and can be expressed as $\Delta V = 2\pi r^2 \Delta r \Delta\theta \sin\theta$. They contribute the amount of emission $\Delta L(\mathrm{r},\theta) = \varepsilon_\alpha \mathrm{n(r)}^2 \Delta \mathrm{V}$ (cf. Eq. 1). Using equations (3) and (4), we can write this as

$$\Delta L(\mathrm{r},\theta) = \xi \frac{\sin(\theta)}{\mathrm{r^2 v(r)^2}} \Delta \mathrm{r} \Delta\theta \quad [\mathrm{erg\,s^{-1}}], \tag{9}$$

where the scaling factor

$$\xi = \frac{\varepsilon_\alpha}{8\pi(\mu m_{\rm H})^2}\dot{M}^2. \tag{10}$$

Integrating all the observable contributions, the calculated luminosity of the line is

$$L = \xi \int_{r_{\rm min}}^{\infty} \int_0^{\theta_{\rm min}} \frac{\sin(\theta)}{r^2 v(r)^2} \mathrm{d}r\mathrm{d}\theta, \tag{11}$$

and redistributing these contributions according to their radial velocities we obtained the resulting profile (Fig. 6). The input parameters, $R_\star$, $r_{\rm min}$ and v_∞, have to be inferred from observations, while the resulting parameters, ξ and β, are given by an appropriate fit to the observed profile.

3.1.3 Application to the active star in CH Cygni

The radius of the star: The temperature and luminosity of the hot component during active phases yield an estimate of the effective radius between about 2.5 and 8 $R_\odot$ (Skopal et al. 1998a). An independent estimate of the hot pseudophotosphere, derived from the geometry of the 1994 eclipse of the active star by its giant companion, provides the value of $4.5 \pm 1.6\,R_\odot$ (Skopal 1997). For the purposes of this paper, we adopt the radius of the active star photosphere in CH Cygni, $R_\star = 5\,R_\odot$.

The inner radius: The minimum radius, $r_{\rm min}$, corresponds to a certain height above the photosphere, at which the optical depth $\tau(\mathrm{H}\alpha) \ll 1$ – a fundamental assumption in our approach. According to Leitherer (1988), for $\dot{M} \approx 10^{-6}\,M_\odot\,\mathrm{yr}^{-1}$, $R_\star = 5\,R_\odot$ and $v(r = 1.5\,R_\star)$, $\tau(\mathrm{H}\alpha)$ is a few $\times 0.01$ for a temperature of the underlying photosphere of 10^4 K (we note, however, that it is very difficult to estimate an accurate value of $T_{\rm eff}$ for the active object in CH Cygni; see Skopal et al. 1998a).

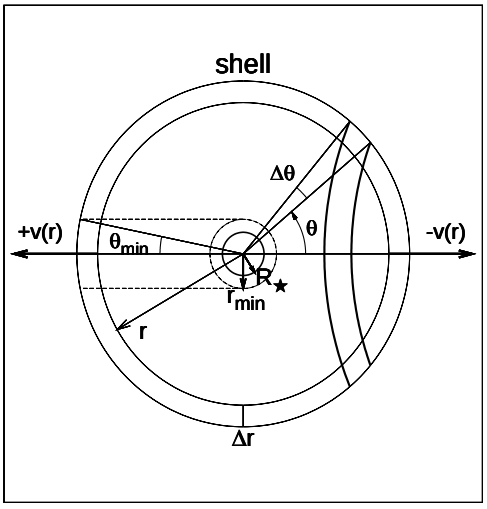

Figure 5. A schematic picture relevant to the text in Sect. 3.1.2, where integration of emission contributions of the spherically symmetric and optically thin wind is described. The belt bounded by the two thick lines represents a part of the shell with the same radial velocity, $-v(r)\cos(\theta)$.

The outer radius: As the integral (11) converges with increasing distance from the central source, we end the integration at a shell at which the wind contributions are negligible. In our case we found such a finite limit to be about 200 $R_\odot$ (Appendix C).

As the resulting profile depends critically on the $r_{\rm min}$ radius, that is not possible to determine firmly, we varied $r_{\rm min}$ in the range of $7 - 9\,R_\odot$ searching for an appropriate value of β, which produced a profile comparable with the observed one (judged by eye). Performing many trials, we found $r_{\rm min} = 8\,R_\odot$ to match the profile in the 5/9/98 spectrogram and $r_{\rm min} = 9\,R_\odot$ for the profiles in the 1984 and 1992 spectra, with corresponding values of the β parameter

$$\begin{aligned} \beta_{1984/92} &= 1.4 \pm 0.2 \\ \beta_{1998} &= 1.9 \pm 0.2. \end{aligned} \tag{12}$$

The uncertainty results from the range of considered values of $r_{\rm min}$. Finally, scaling the calculated profile to the maximum of the observed 'wind' component(s) we also obtained the factor ξ. In Fig. 6 we compare resulting calculated profiles to observations. Variation in the line profile with β is shown in the mid-top panel of Fig. 6. In spite of strong simplification of our approach (e.g. no effects of radiative transfer in the line were included) one can see that the modelled profiles match basic features of the observed wind components: (i) The very extended bases of the profiles, which are due to contributions from far distances from the star, where $v(r) \sim v_\infty$ and the wind density is low. (ii) The asymmetry of the profiles with respect to the reference wavelength. The maxima are blueward shifted. This effect results from the fact that a fraction of the radiation produced by the wind

Table 3. Mass-loss rates from Hα

Date	$L^\star$ $[L_\odot]$	v_∞ $[\mathrm{km\,s^{-1}}]$	β	I_w	$\dot{M}$ $[10^{-6}\,M_\odot\,\mathrm{yr}^{-1}]$
4/10/84	2.25	3 500±500	1.4±0.2	1.5±0.3	4.4±1.5
11/8/92	2.11	2 500±500	∼1.4	∼1.5	∼2.0
5/9/98	2.34	3 000±300	1.9±0.2	4.0±1.0	1.8±0.7

* For the observed fluxes in Table 2 and the distance of 270 pc

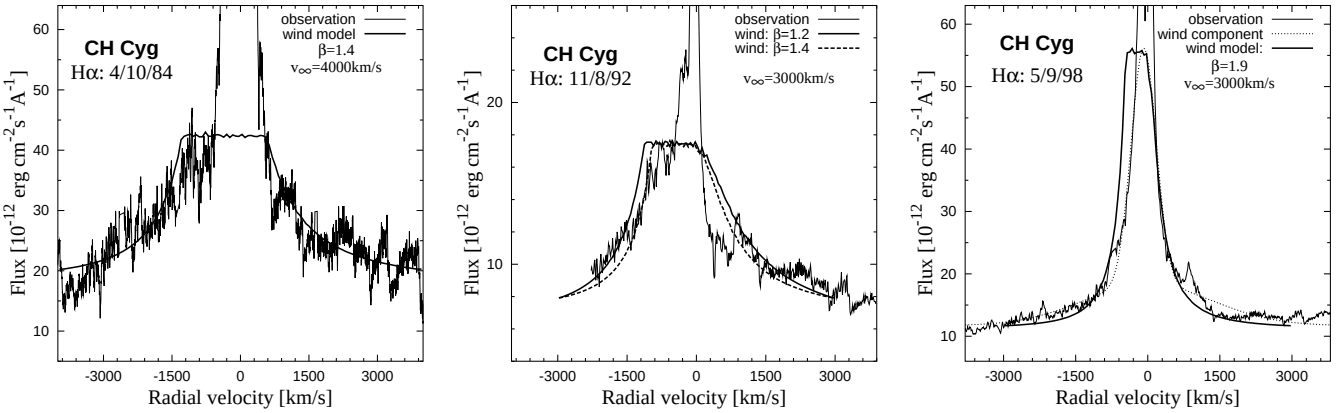

Figure 6. Comparison of the modelled profiles of Hα formed in an optically thin spherically symmetric stellar wind and the 'wind' components of the observed profiles. This allows us to estimate the β parameter in the wind law (Eq. 4)

is occulted by the star and the optically thick inner regions $\lesssim r_\mathrm{min}$.

According to parameters $L(\mathrm{H}\alpha)$, v_∞, determined from observations, and parameters β, I_w derived from modelling the line profiles, with the aid of Eq. (5), we determined the mass-loss rate from the active star

$$\dot{M}_{1984} = (4.4 \pm 1.5) \times 10^{-6} M_\odot\,\mathrm{yr}^{-1}$$
$$\dot{M}_{1998} = (1.8 \pm 0.7) \times 10^{-6} M_\odot\,\mathrm{yr}^{-1}. \quad (13)$$

The results are summarised in Table 3. Uncertainties in the $\dot{M}$ values were determined from those of $L(\mathrm{H}\alpha)$, v_∞ and I_w (converted from β). Special attention was payed to estimate the uncertainty in the $H\alpha$ fluxes. Including the uncertainty given by our calibration method of the spectra ($\sim 20\%$) and that caused by the contribution of the late-type spectrum to the $H\alpha$ emission ($\sim 20\%$), we estimated the total uncertainty of the $H\alpha$ fluxes to about 40% (Appendix B). As the mass loss rate is proportional to $\dot{M} \propto \sqrt{(L(H\alpha))}$ (Eq. 5), the larger uncertainty in fluxes increases that of $\dot{M}$ with only square root.

In principle, the mass loss rate could be also estimated from fitting the line profiles. However, the calculated profiles imply uncertainties, so we do not use our line-profile fitting procedure to determine $\dot{M}$, but only to estimate the parameter β.

4 DISCUSSION

In this section we briefly discuss some properties of the investigated mass outflow in CH Cyg, which are connected with our simplified model.

4.1 Comparison with $\dot{M}$ determined in the radio

Here we compare our Hα mass-loss rates with those obtained from radio observations. From the 1984 radio images, Taylor, Seaquist & Mattei (1986) derived a mass-loss rate of $\dot{M} > 7 \times 10^{-6}\,M_\odot\,\mathrm{yr}^{-1}$ for a distance of 400 pc. Their estimate is based on the appearance of an additional emission component at a time <75 days (between 8/11/84 and 22/1/85). Its size and particle density then yield its mass. As this estimate is distance dependent with $\dot{M} \propto d^{1/3}$, the distance of 270 pc reduces it to $\dot{M} > 2.2 \times 10^{-6}\,M_\odot\,\mathrm{yr}^{-1}$. From the radio data obtained in 1992 and 1993, Skopal et al. (1996b) inferred an expansion velocity of $(3\,000 \pm 400) \times D_\mathrm{kpc}\,\mathrm{km\,s^{-1}}$ and a mass-loss rate of $\dot{M} = (7.8 \pm 1.2) \times 10^{-6}\,M_\odot\,\mathrm{yr}^{-1}$ for $d =$ 400 pc, which scales to $\dot{M} = (2.8 \pm 0.4) \times 10^{-6}\,M_\odot\,\mathrm{yr}^{-1}$ for d = 270 pc. This very good agreement between both independent findings of the mass-loss rate in CH Cyg demonstrates the reliability of our approach. This is important, because radio mass-loss rates are less model dependent than the Hα method. In the former case we observe the ejected material at very large distances from the star (from a few 10's of A.U. to ≈1 000 A.U.), where a constant expansion velocity can be reliably assumed. On the other hand, in the latter approach we are dealing with regions at distances of a few $R_\odot$ to, at maximum, a few hundreds of $R_\odot$, the emissivity of which critically depends on the velocity law, whose structure, however, has to be assumed. In principle, high-resolution Hα spectroscopy could yield density and velocity information (Olson & Ebbets 1981), but it requires a precise synthetic-line profile fitting that is quite ambiguous (Leitherer 1988).

4.2 Mass loss as a transient phenomenon

The high-velocity mass loss in CH Cyg is connected only with the active phases of type (1). This is suggested, for example, by the evolution of the radio light curves presented by Kenny et al. (1996) for the period 1984 April to 1995 August. Also the mass flow during type (1) activity correlates with the star's brightness in U. A dependence of the Hα luminosity on the level of U magnitude, which is considered to measure the activity in the system, was shown by Bode et al. (1991) for the period of 1986 to 1990. The brighter the system, the higher the Hα emission. A correlation of the same type, but for the radio emission, can be easily deduced from 1986 to 1999 VLA images presented by Crocker et al. (2001). On the other hand, during the maximum of the star's brightness (type 2), the radio flux was very low (see Fig. 1 of Taylor et al. 1986), which is in agreement with the fact that no significant mass outflow could be identified in the optical.

4.3 Irregular mass loss

According to numerous spectroscopic observations made in the optical, the mass outflow in CH Cyg was highly irregular. Only during 1984.6-87, a more or less continuous flow with a decreasing trend of terminal velocity and the amount of emission, was detected (Hack et al. 1988). A typical feature of the irregularity in the mass outflow during 1992-95 and 1998-00, was a sudden emergence of a (strong) blueward shifted absorption propagating in the emission wing to $\sim$-1 000 km s^{-1}on a time-scale of days (Fig. 3, Tomov et al. 1996, Skopal et al. 1996b). As a result the profile has a complex emission/absorption structure, which does not allow one to apply easily our simplified model. For example, it is very difficult to determine the total emission from the wind only (see e.g. Fig. 3 right panels), and mainly, the height above the pseudophotosphere, where the mass flow becomes optically thin (i.e. the parameter r_{min} in our model). Therefore we had to select a spectrum with a simple broad emission as was observed, for example, on 5/9/1998 in which parameters of the model (Sect. 3.1.3) and the flux of the wind component of radiation can be determined. From this point of view, the derived mass-loss rate in 1998 represents an average value for this active phase.

In some cases we observed absorptions redward of the reference line as a counterpart to their more pronounced blueward absorptions (Fig. 3). The inflow of matter could possibly be a result of the wind compressed disk creating around mass losing rapidly rotating stars (Bjorkman & Cassinelli 1993). In such a model there is a stagnation point in the disk where the radial flow is zero. In the inner region in the disk, below the stagnation radius, material re-accretes back onto the star (Owocki, Cranmer & Blondin 1994). This interesting feature of the CH Cygni phenomenon is worthy of a detailed analysis in a future paper.

4.4 Deceleration of the ejected material

A deceleration of the ejected material in CH Cyg is evident from comparison of the optical and radio observations. At optical wavelengths we observe terminal velocities around 3 000 km s^{-1}, while the evolution of the ejecta in radio maps suggests an expansion velocity of $\leq$ 1 000 km s^{-1}as we noted in section 4.1. Generally, this effect results from interaction of the flow – originally accelerated to $\approx$ 3 000 km s^{-1}at a distance of $\sim 100\,R_\odot$ – with the interstellar medium at distances of hundreds A.U. that decelerates it to about 1 000 km s^{-1}(as was observed in 1984-5 and 1991-93). Later, in the HST optical image taken on 1/10/1999, Corradi et al. (2001) found that expansion velocities could be as low as $\sim$100 km s^{-1}. In both periods (1984.6-85, 1998-00) the flow is accelerated to approximately the same v_∞ (Fig. 3), but decelerated to different values. As the position of the system with respect to the observer (i.e. the orbital phase of the outer binary, φ) is practically the same in 1984-85 and 1999 ($\varphi \sim 0$, see position of eclipses in the outer binary in the light curve in Fig. 1), this cannot be due to a different projection of the flow to the sky. The effect of an increasing deceleration thus probably results from the density increase in the decelerating medium around CH Cygni. As time progresses the amount of material swept up by originally freely expanding wind increases and the momentum of the wind cannot drive the shell in front of it to such high speed. Thus the shell slows down (Castor, McCray & Weaver 1975). However, a quantitative model to determine the velocity, density and temperature structure of the ejected material as a function of the radial distance is needed to elaborate to understand better the CH Cygni ejecta given by the observations of Crocker et al. (2001), Corradi et al. (2001) and Eyres et al. (2002).

5 CONCLUSIONS

(i) We have summarized basic characteristics that are common for active phases during the whole (1963-2000) observed symbiotic life of CH Cygni. We identified two basic types of activity with respect to the dominance of (1) a *mass outflow* from and (2) a *mass inflow* to the central star. According to this scheme, high-velocity outflows dominated the main spectroscopic features of the active phases, 1967-70, 1984.6-88, 1992-95 and 1998-00, while during the maximum in 1977-84.6, they reflected a mass infall.

(ii) On the basis of the Hα emission, we derived mass loss from the active star during the period after the radio jets' appearance (1984.6) to the time of the most recent activity (1998-00). Based on a simple expression, which relates the observed Hα luminosity to the mass-loss rate, we obtained $\dot{M} = 4.4 \pm 1.5$, $\approx$ 2.0 and $1.8 \pm 0.7 \times 10^{-6}\,M_\odot\,\mathrm{yr}^{-1}$ in 1984 October, 1992 August and 1998 September, respectively. Our values agree well with mass-loss rates derived from radio observations.

(iii) Mass loss from CH Cygni is a transient effect connected only with active phases of type (1), and it is highly variable.

(iv) Our optical spectroscopy revealed that the ejected material was accelerated approximately to the same terminal velocity, $v_\infty \approx$3 000 km s^{-1}, during all investigated periods (1984.7, 1992.6, 1998.7). On the other hand, radio and most recently also the HST and ground-based optical images suggest velocities up to one order of magnitude lower.

Acknowledgments

This research was supported by a grant SLA/1039115 of the Alexander von Humboldt foundation and in part by a grant of the Slovak Academy of Sciences No. 1157. AS acknowledges the hospitality of the Astronomisches Institut der Universität Erlangen-Nürnberg in Bamberg and of the Astrophysics Research Institute of the Liverpool John Moores University.

REFERENCES

Anderson M.Ch., Oliversen N.A., Nordsieck K.H., 1980, ApJ, 242, 188
Bjorkman J.E., Cassinelli J.P., 1993, ApJ, 409, 429
Bode M.F., Roberts J.A., Ivison R.J., Skopal A., 1991, MNRAS, 253, 80
Castor J.I., Abbott D.C., Klein R.I., 1975, ApJ, 195, 157
Castor J.I., McCray R., Weaver R., 1975, ApJ, 200, L107
Corradi R.L.M., Munari U., Livio M., Mampaso A., Goncalves D.R., Schwarz H.E., 2001, ApJ, 560, 912
Crocker M.M., Davis R.J., Eyres S.P.S., Bode M.F., Taylor A.R., Skopal A., Kenny H.T., 2001, MNRAS, 326, 781
Deutsch R.J., 1964, Ann. Rep. Mt. Wilson and Palomar Observatories, p.11
Doan N., 1970, A&A, 8, 307
Eyres S.P.S., Bode M.F., Skopal A., Crocker M.M., Davis R.J., Taylor A.R., 2002, submitted to MNRAS
Faraggiana R., Hack M., 1971, A&A, 15, 55
Fernie D., Lyons R.,Beattie B., Garrison R.F., 1986, IBVS No. 2935
Gurzadyan G.A. 1997, The Physics and Dynamics of Planetary Nebulae, Sprinfer-Verlag, p. 60
Hack M., et al., 1986, A&A, 159, 117
Hack M., et al., 1988, A&AS, 72, 391
Hauschildt P.H., Allard F., Ferguson J., Baron E., Alexander D.R., 1999, ApJ, 525, 871
Henden A.A., Kaitchuck R.H., 1982, Astronomical Photometry, Van Nostrand Reinhold Company, New York, 50
Hinkle K.H, Fekel F.C., Johnson D.S., Scharlach W.W.G., 1993, AJ, 105, 1074
Iijima T., 1998, MNRAS, 297, 77
Kenny, H.T. et al., 1996, ASP Conference Series, 93, 197
Klein R.I., Castor J.I., 1978, ApJ, 220, 902
Lamers H.J.G.L.M., Cassinelli L.P., 1999, Introduction to Stellar Winds, CUP, Cambridge
Leitherer C., 1988, ApJ, 326, 356
Mikolajewski M., Tomov T., 1986, MNRAS, 219P, 13
Mikolajewski M., Mikolajewska J., Tomov T., 1987, Ap&SS, 131, 733
Mikolajewski M., Mikolajewska J., Khudyakova T.N., 1990, A&A, 235, 219
Mikolajewski M., Tomov, T.V., Kolev D., Leedjärv L., 1996, IBVS No. 4368
Mikolajewski M., Leedjärv L., 1998, IAU Circ. 6967
Olson G.L., Ebbets D., 1981, ApJ, 248, 1021
Owocki S.P., Cranmer S.R., Blondin J.M., 1994, ApJ, 424, 887
Skopal A., 1986, Bull. Astron. Inst. Czechosl. 37, 18
Skopal A., 1995, IBVS No. 4157
Skopal A., 1997, In: J. Mikolajewska (ed.), Physical processes in symbiotic binaries, Copernicus Foundation for Polish Astronomy, p. 99
Skopal A., 2001, A&A, 366, 157
Skopal A., Mikolajewski M., Biernikowicz R., 1989, Bull. Astron. Inst. Czechosl. 40, 333
Skopal A., Hric L., Komžík R., 1992, IAU Circ. 5504
Skopal A., Chochol D., Komžík R., In: A.Vittone and L.Errico (eds.), Stellar jets and bipolar outflows. Kluwer Acad. Publishs, Dordrecht, Holland, 1993, p. 163
Skopal A., Bode M.F., Lloyd H.M., Tamura S., 1996a, A&A, 308, L9
Skopal A., Bode M.F., Bryce M. et al., 1996b, MNRAS, 282, 327
Skopal A., Bode M.F., Lloyd H.M., Drechsel H., 1998a, A&A, 331, 179
Skopal A., Bode M.F., Lloyd H.M., Drechsel H., 1998b, A&A, 331, 224
Skopal A., Pribulla, T., Wolf, M., Shugarov, S.Y., Jones, A., 2000, Contrib. Astron. Obs. Skalnate Pleso, 30, 29
Taranova O.G., Yudin B.F., 1988, Ap&SS, 146, 33
Taranova O.G., Yudin B.F., Kolotilov E.A., 1995, Astron. Let., 21, 470
Taranova O.G., Shenavrin, V.I., 2000, Astron. Rep., 44, 460
Taylor A.R., Seaquist E.R., Mattei J.A., 1986, Nat. 319, 38
Tomov T., Kolev, D., Munari, U., Antov, A., 1996, MNRAS, 278, 542
Viotti R., Badiali M., Cardini D., Emanuele A., Iijima T., 1997, in B. Batrick (ed.), *Hipparcos* Venice 1997, ESA-SP-402, Esa Publ., Nordwijk, p. 405
Vogel M., 1993, A&A, 274, L21
Vogel M., Nussbaumer H., 1994, A&A, 284, 145
Yamashita Y., Maehara M., 1979, PASJ, 31, 307

APPENDIX A: FLUX CALIBRATION OF THE SPECTRA

In this appendix we describe our method of flux calibration of the spectra we used to estimate the mass loss rate. This is particularly important to determine the Hα fluxes.

First, we summarized photometric observations from the literature carried out (nearly-)simultaneously with the spectrum under consideration. Then we converted the observed magnitudes to fluxes according to the calibration of Henden & Kaitchuck (1982). No reddening was applied (Sect. 4.1 of Skopal et al. 1996b). Table A1 gives the $UBVR$ calibration for three dates, at which we estimate the mass-loss rate. Second, we determined the star's continuum by fitting the $UBVR$ fluxes with a 3-order polynomial function. Finally, we scaled the measured spectrum to this fit and thus obtained it in units of erg cm^{-2} s^{-1} Å^{-1}. Figure A1 shows an example of such a calibrated spectrum from 5/9/1998. According to this method the uncertainty in the Hα flux is therefore essentially limited by that of the R-band flux. The fluxes listed in Table A1 represent average values of photometry taken around the spectroscopic observations, because no exactly simultaneous photometric observation was available. We can see that the uncertainties do not exceed about 25% in R. As the S/N ratio of our high-resolution spectra is about 100, (or larger for the CCD spectra), we did not consider their intrinsic uncertainties, which probably amount to only a few percent.

APPENDIX B: INFLUENCE OF THE LATE-TYPE SPECTRUM ON THE Hβ AND Hα PROFILES

Here we comment on the influence of the late-type spectrum of CH Cygni on the Hβ and Hα profiles taken in 1992 August and 1984 October, when its contribution was most

Table A1. Flux calibration to spectra in Figure 3

Date	JD-2 400 000	$U/F_{\rm U}$	$B/F_{\rm B}$	$V/F_{\rm V}$	$R/F_{\rm R}$	Ref.
			[mag/10^{-12} erg cm^{-2} s^{-1} Å^{-1}]			
04/10/84	45 978	6.8±0.3/8.3±2.3	7.3±0.1/8.6±1.8	6.8±0.1/7.5±0.7	4.5±0.2/28±5.1	1, 2
11/08/92	48 846	8.1±0.2/2.5±0.5	8.9±0.2/2.0±0.4	8.2±0.1/2.1±0.2	5.2±0.2/13±2.5	3, 4
05/09/98	51 063	8.1±0.2/2.5±0.5	8.5±0.2/2.9±0.5	7.8±0.2/3.1±0.5	4.8±0.2/21±3.9	5, 6

1 - Bode et al. (1991), 2 - Mikolajewski, Mikolajewska & Khudyakova (1990), 3 - Taranova et al. (1995), 4 - Mikolajewski et al. (1996), 5 - Skopal et al. (2000), 5 - Mikolajewski & Leedjärv (1998)

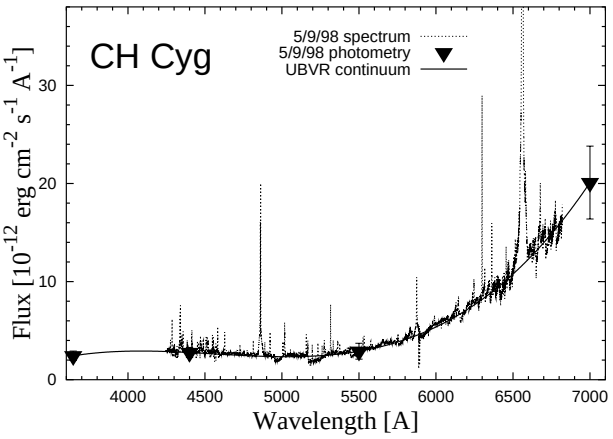

Figure A1. Spectrum of CH Cygni on 5/9/98 calibrated to the nearly-simultaneous broad-band $UBVR$ photometry. The solid line represents the calculated continuum.

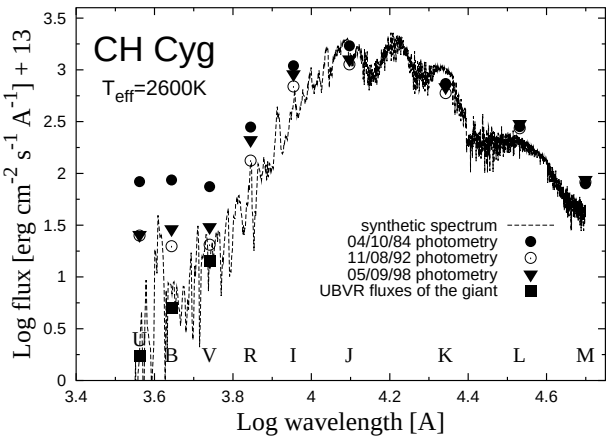

Figure B1. Spectral energy distribution of CH Cygni represented by the broad-band optical and infrared $UBVRI$ and $JKLM$ photometry for three dates, at which we estimate the mass-loss rate. A synthetic spectrum of $T_{\rm eff}$ = 2 600 K matches the UBV fluxes of the red spectrum (cf. Table 6 of Skopal et al. 1996b) and the observed fluxes in I, J and K bands. An emission excess in L and M bands is due to dust (Taranova & Shenavrin 2000). The synthetic spectrum was selected from a grid of cool giant spectra shown by Hauschildt et al. (1999) and infrared photometry from the data published by Taranova & Yudin (1988), Taranova & Shenavrin (2000) and references in Table A1.

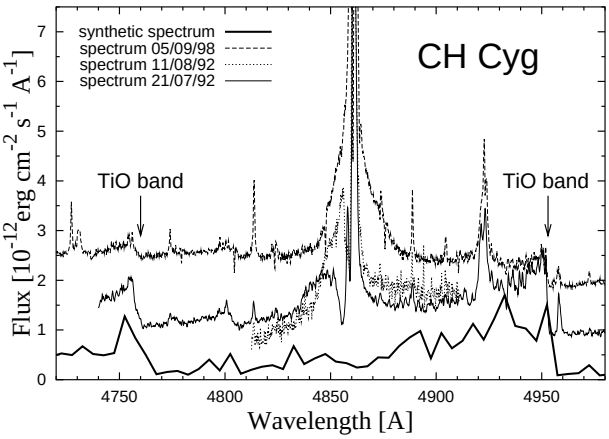

Figure B2. Comparison of the observed spectra around the Hβ line with the synthetic giant's spectrum.

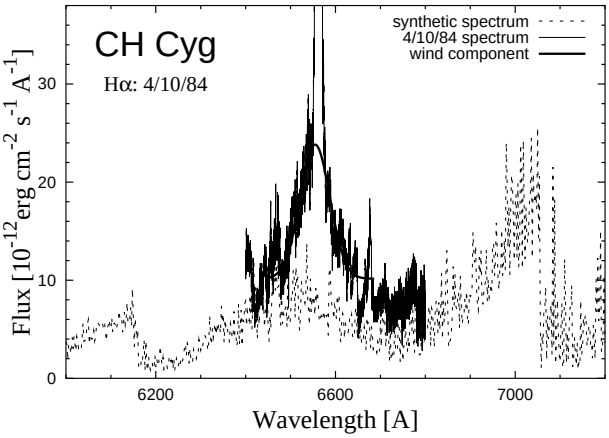

Figure B3. Comparison of the observed spectrum around the Hα line with the synthetic giant's spectrum. This confirms the reality of very extended emission wings of the Hα profile. However, the influence of the red spectrum enlarges the uncertainty in the Hα flux by about 20%.

pronounced (see Fig. 3). This is important mainly to determine the wide emission wings supposed to originate from the hot star wind.

First, we matched the UBV fluxes of the red spectrum and the observed fluxes in the I, J and K bands by a synthetic giant's spectrum of $T_{\rm eff}$ = 2 600 K (see Fig. B1). However, the situation is very complicated due to the large variability of the giant's spectral type (from M5 to M7-8; e.g. Bode et al. 1991) and/or dust emission in the system depending on the activity (e.g. Taranova & Yudin 1988, Tara-

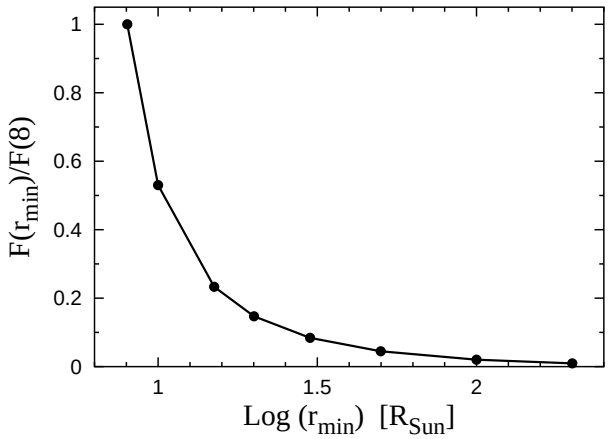

Figure C1. Ratio of line fluxes $F(r_{\rm min})/F(8)$ calculated according to equation (11). $F(8)$ represents the line flux ($\rm erg\,cm^{-2}\,s^{-1}$) for $r_{\rm min} = 8\,R_\odot$. This demonstrates that contributions beyond $200\,R_\odot$ from the central source are less than 1% of the total flux.

nova & Shenavrin 2000). As a result, it is not possible to select a synthetic spectrum which fits all the observed broadband photometric fluxes. Therefore our comparison represents only an average spectral energy distribution for the considered three observing epochs.

Second, we compared the theoretical spectrum around Hβ and Hα lines to observations. Figure B2 shows the Hβ region. An apparent gradient of the continuum of the giant between TiO 4755 and TiO 4952 makes the observed continuum level on the red side of Hβ higher than on the blue side. Such influence of the M spectrum makes it difficult to fit the broad emission wing of Hβ during the 1992 active phase (Sect. 3, Table 2). Figure B3 then shows comparison of the synthetic spectrum with our observation on 4/10/84 in the region around Hα. It is evident that extended emission wings of the Hα line of the active component are present. However, it is not possible to disentangle its contribution from the late-type spectrum, because of uncertain calibration of the synthetic spectrum as mentioned above. This fact enlarges the uncertainty of our flux determination by a (symmetrical) Gaussian function by about 20%.

APPENDIX C: THE OUTER RADIUS OF THE WIND EMISSION REGION

In this appendix we demonstrate a dependence of the wind emission on the radial distance r. This is important to determine the outer radius of the wind contributions to integrate Eq. (11).

As the emission contributions to the line are proportional to the radial distance as r^{-2}, contributions to the total line flux are a strong function of the radial distance. Figure C1 shows the line fluxes as a function of the $r_{\rm min}$ radius calculated according to equation (11). This shows that about 99% of the wind emission in the optical comes from regions in between the distances $8\,R_\odot$ and $150\,R_\odot$. In this way we clarify our statement in section 3.1.3 on a finite outer radius of about $200\,R_\odot$, beyond which emission contributions are negligible.